Photo-inducible cell ablation in *Caenorhabditis elegans* using the genetically encoded singlet oxygen generating protein miniSOG

Yingchuan B. Qi[a,1], Emma J. Garren[a], Xiaokun Shu[b,c], Roger Y. Tsien[c,d,2], and Yishi Jin[a,d,2]

[a]Division of Biological Sciences, Neurobiology Section, University of California, San Diego, CA 92093; [d]Howard Hughes Medical Institute, University of California, San Diego, CA 92093; [b]Department of Pharmaceutical Chemistry, University of California, San Francisco, CA 94158; and [c]Department of Pharmacology, University of California, San Diego, CA 92093

Contributed by Roger Y. Tsien, March 9, 2012 (sent for review January 5, 2012)

We describe a method for light-inducible and tissue-selective cell ablation using a genetically encoded photosensitizer, miniSOG (mini singlet oxygen generator). miniSOG is a newly engineered fluorescent protein of 106 amino acids that generates singlet oxygen in quantum yield upon blue-light illumination. We transgenically expressed mitochondrially targeted miniSOG (mito-miniSOG) in *Caenorhabditis elegans* neurons. Upon blue-light illumination, mito-miniSOG causes rapid and effective death of neurons in a cell-autonomous manner without detectable damages to surrounding tissues. Neuronal death induced by mito-miniSOG appears to be independent of the caspase CED-3, but the clearance of the damaged cells partially depends on the phagocytic receptor CED-1, a homolog of human CD91. We show that neurons can be killed at different developmental stages. We further use this method to investigate the role of the premotor interneurons in regulating the convulsive behavior caused by a gain-of-function mutation in the neuronal acetylcholine receptor *acr-2*. Our findings support an instructive role for the interneuron AVB in controlling motor neuron activity and reveal an inhibitory effect of the backward premotor interneurons on the forward interneurons. In summary, the simple inducible cell ablation method reported here allows temporal and spatial control and will prove to be a useful tool in studying the function of specific cells within complex cellular contexts.

light inducible | locomotion | optogenetics | reactive oxygen species | pre-motor interneurons

Tools that allow for selective ablation of cells in a temporally and spatially precise manner have greatly facilitated our ability to dissect the function of a cell within a complex network such as the nervous system. Genetically encoded cell ablation reagents are highly desirable, as they can be used in combination with a variety of cellular manipulations. Key enzymes in programmed cell-death pathways, such as caspases (1), and cytotoxic molecules, such as gain-of-function mutant degenerins (2) or diphtheria toxin A (3, 4), are commonly used reagents to kill cells. However, these cell ablation methods rely on constitutive expression of such reagents, and the efficiency of cell ablation can vary depending on the cell type, physiological state, and possibly other factors. Several conditional cell ablation methods have also been reported and are primarily based on the combinatorial activity of exogenous immunotoxin or chemicals (5–8). For example, transgenic expression of *Escherichia coli* nitroreductase in zebrafish can ablate cells upon conversion of the prodrug metronidazole into a cytotoxic DNA cross-linking agent (6, 7). Targeted expression of the human interleukin 2 receptor α-subunit in mice can cause inducible cell killing upon binding of a recombinant immunotoxin (5). Developing additional inducible cell-killing methods will offer versatility to the toolbox for cellular manipulations.

Recent technological developments have identified exogenous photosensitizers that release reactive oxygen species (ROS) upon light excitation. Photo-inducible cell killing exploits the ability of ROS to potentially damage any macromolecules within the cell by over-oxidation; when the oxidative stress reaches a certain threshold, cell death ensues (9). Chemically based photosensitizing reagents have been used in photodynamic therapy, a clinically approved, minimally invasive procedure to kill malignant cells (10). Once administered, however, these chemical photosensitizers may accumulate in tissues other than cancerous cells, causing non-specific toxicity. Genetically encoded photosensitizers enable more selective targeting and can offer a unique way to investigate cellular function in a site- and stage-specific manner (11–14). However, fully genetically encoded and functionally effective photosensitizers remain scarce. A promising photosensitizer recently reported is KillerRed, which generates ROS upon irradiation with green light and can ablate cells when targeted to mitochondria in cultured mammalian cells (12) or when targeted to plasma membrane in zebrafish (14). However, KillerRed is a relatively large protein and requires dimerization for its phototoxicity, which may impose limitations for efficient expression.

MiniSOG (mini singlet oxygen generator) is a green fluorescent flavoprotein engineered from *Arabidopsis* phototropin 2 (15). miniSOG consists of 106 amino acids and acts as a monomer. Upon blue-light illumination, miniSOG generates a sufficient quantity of singlet oxygen and has been shown to effectively catalyze local polymerization of diaminobenzidine into precipitates for imaging using electron microscopy (15). Here, we took advantage of the ROS-producing property of miniSOG and demonstrated that mitochondrially targeted miniSOG is a potent light-induced cell-ablation reagent in *Caenorhabditis elegans*. We also provide examples of the use of this method in studying neural function.

Results

Mitochondrially Targeted miniSOG Kills Cells After Blue-Light Illumination. To explore the use of miniSOG in cell killing, we designed a series of transgenic expression constructs targeting miniSOG to subcellular locations (Fig. 1*A*; Table S1). Because mitochondria are prone to the damaging effects of oxygen radicals and play key roles in the regulation of cell death (9), we tagged miniSOG using a number of mitochondrial protein-targeting sequences (16). We previously reported the use of the N-terminal 29-amino-acid residues of human COX8a (cytochrome *c* oxidase subunit VIIIA) to target miniSOG to the mitochondrial matrix (15). To target miniSOG onto the outer mitochondrial membrane, we fused miniSOG to the C terminus of TOMM-20, the *C. elegans* ortholog of human TOM20, the major receptor for the import of polypeptides into mitochondria (17). We also used the N-terminal 55-amino-acid residues of TOMM-20 to target miniSOG, as this

Author contributions: Y.B.Q., X.S., R.Y.T., and Y.J. designed research; Y.B.Q. and E.J.G. performed research; X.S. and R.Y.T. contributed new reagents/analytic tools; Y.B.Q., E.J.G., and Y.J. analyzed data; and Y.B.Q., E.J.G., R.Y.T., and Y.J. wrote the paper.

The authors declare no conflict of interest.

Freely available online through the PNAS open access option.

[1]Present address: Institute of Developmental and Regenerative Biology, Hangzhou Normal University, Hangzhou 310036, China.

[2]To whom correspondence may be addressed. E-mail: rtsien@ucsd.edu or yijin@ucsd.edu.

This article contains supporting information online at www.pnas.org/lookup/suppl/doi:10.1073/pnas.1204096109/-/DCSupplemental.

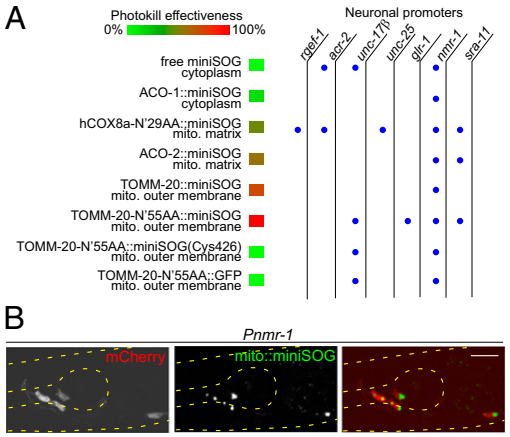

Fig. 1. Specific neuronal ablation by light-activated mitochondrially targeted miniSOG. (*A*) miniSOG constructs and the effectiveness of cell ablation. The neuronal promoters are described in Table S2. *rgef-1*, pan-neurons; *acr-2*, A- and B-type cholinergic motor neurons; *unc-17β*, A- and B-type cholinergic motor neurons; *unc-25*, D-type GABAergic motor neurons; *glr-1*, premotor interneurons, a subset of head motor neurons and interneurons; *nmr-1*, a subset of premotor interneurons and RIM; *sra-11*, premotor interneurons AVB and interneurons AIA and AIY. Blue dots indicate that the transgene of miniSOG constructs driven by the corresponding neuronal promoters was tested. (*B*) Green fluorescence of *mito-miniSOG* is visible in soma when expressed in *Pnmr-1*-cells, which are colabeled by mCherry. (Scale bar, 10 μm.)

polypeptide was shown to localize GFP to mitochondria (18). Because an important mechanism underlying ROS toxicity appears to involve direct oxidation and inactivation of iron–sulfur proteins, such as mitochondrial aconitases (19), we also tagged miniSOG at the C terminus of ACO-2, the mitochondrial aconitase in *C. elegans*, as well as at the C terminus of ACO-1, the cytoplasmic aconitase (20). These miniSOG constructs were expressed using several neuron-type specific promoters (Fig. 1*A*; Tables S1 and S2). Under blue-light illumination, cells expressing free miniSOG showed diffuse green fluorescence that photobleached rapidly, whereas the various mitochondrially targeted miniSOG constructs showed green fluorescence primarily concentrated in cytoplasm of the neuronal cell body (Fig.1*B*), likely reflecting the relatively high concentration of mitochondria in the soma. When cultured under typical indoor illumination (~0.2 mW/cm^2), the transgenic animals expressing free miniSOG or mitochondrially targeted miniSOG in various types of neurons did not display any obvious behavioral defects (Table S1 and Movie S1), and neuronal morphology was grossly normal (Figs. 2*A* and 3*A* and *B*), indicating that miniSOG does not cause discernible toxicity under standard *C. elegans* culture conditions.

To test if activation of miniSOG could result in cell ablation, we exposed freely moving transgenic animals under wide-field blue light (475 ± 20 nm) at an intensity of 57 mW/cm^2 for 30 min using an epi-fluorescence compound microscope (*Materials and Methods* and *SI Materials and Methods*). Under the tested conditions, free miniSOG did not induce detectable effects, whereas all mitochondrially targeted miniSOG caused animals to exhibit behavioral deficits to variable degrees within 30 min after illumination (Fig.1*A*; Table S1). To visualize the morphological effects on the targeting neurons, we coexpressed mCherry under the corresponding promoters for mito-miniSOG. Within a few hours post light illumination, mCherry-labeled cells began to show shape changes, including rounding up, shrinkage, vacuolation, and swellings in the soma and neuronal processes (Fig. 2*A*). By 16 h, the mCherry fluorescence in cell bodies had disappeared, and neuronal processes appeared to have disintegrated (Fig. 2*B*). Using Nomarski differential interference contrast (DIC) microscopy, we inspected the nuclei of the targeting neurons and confirmed that disappearance of mCherry was indeed correlated with absence of the cells (Fig. 3*A*). It is

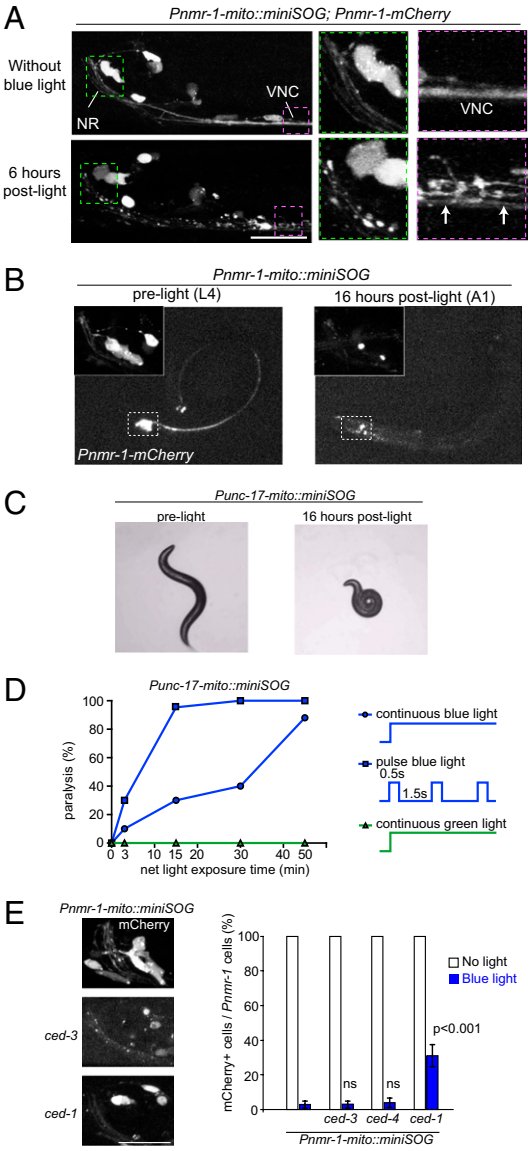

Fig. 2. Time course and light dose of cell ablation by activated mito-miniSOG. (*A*) Dying cells following photo-activation of *mito-miniSOG*. Shown are confocal images of the head region (NR, nerve ring) and anterior ventral nerve cord (VNC) of the animals 6 h after blue-light exposure. In green and pink dotted frames are the blow-up views of the same worm. Dying cells viewed by mCherry show swelling of soma and fragmentation of nerve bundles of VNC (arrows). (Scale bar, 10 μm.) (*B*) Light-induced cell ablation in transgenic *Pnmr-1-mito-miniSOG* animals 16 h post light illumination. (*Insets*) Enlarged views of mCherry in *Pnmr-1* neurons before light illumination and disappearance of mCherry-labeled cells. (*C*) Ablation of *Punc-17β*–expressing cells (DA, DB, VA, and VB motor neurons) by *mito-miniSOG* causes paralysis. (*D*) The graph shows that light dosage correlates with the percentage of paralysis induced by mito-miniSOG upon illumination under continuous or pulsed light. A total of 20–30 animals were analyzed for each data point. (*E*) Ablation of *Pnmr-1* cells by mito-miniSOG is independent of *ced-3* or *ced-4*; the clearance of damaged cell bodies and processes is partially blocked by *ced-1*. A total of 20–40 animals of each genotype were analyzed. (Scale bar, 10 μm.) Statistics used two-tailed Student's *t* test. Error bar shows SEM. Data for *ced-3*, *ced-4*, and *ced-1* are compared with the data for the same transgene in wild-type background.

worth noting that the mCherry marker provided further measure that the ablation resulted in a complete disintegration of the dying cells. Under parallel blue-light illumination, transgenic animals expressing mitochondrially targeted GFP or mCherry

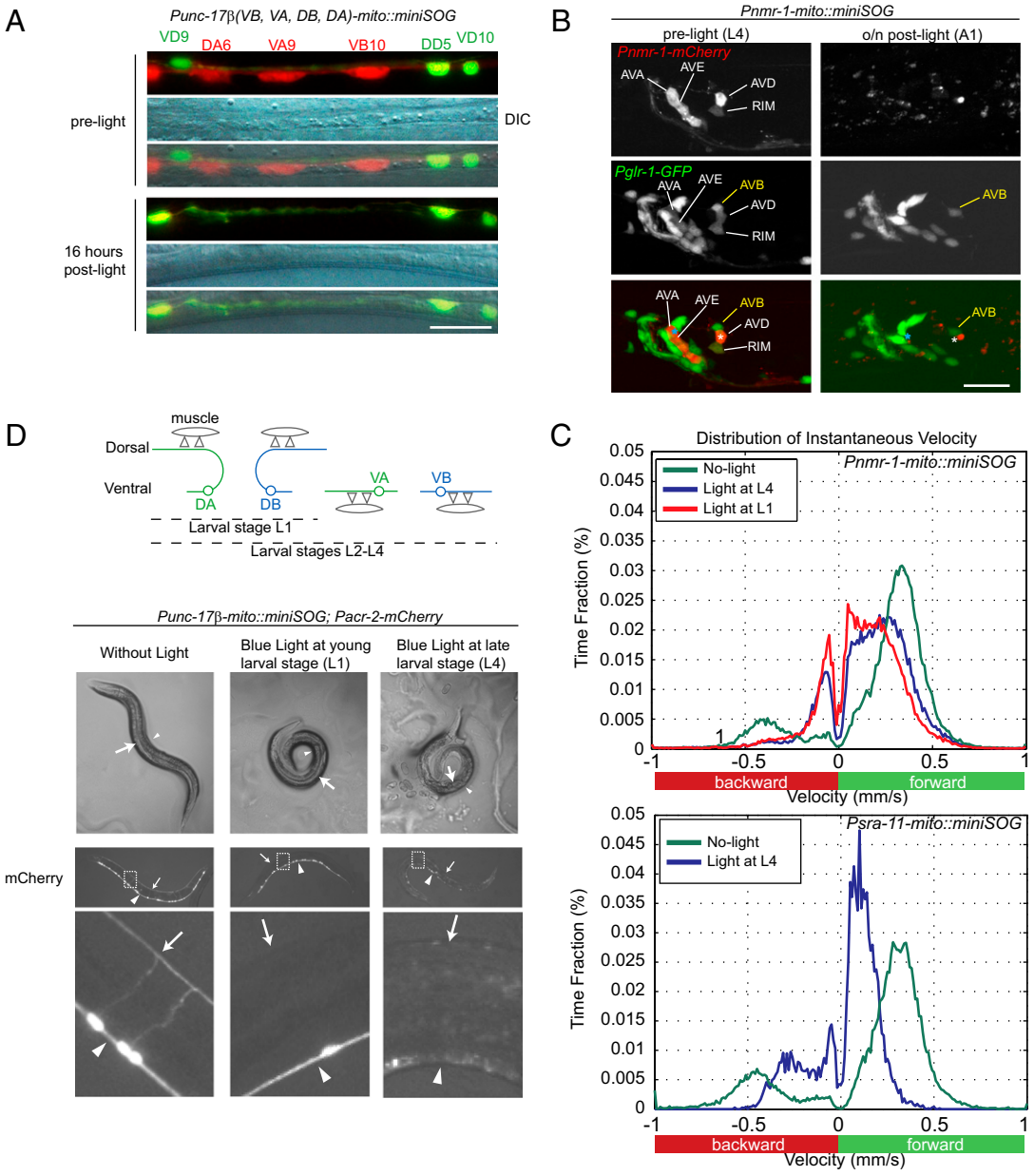

Fig. 3. Activation of mito-miniSOG confers no detectable nonautonomous cytotoxicity and can be induced temporally. (*A*) Photokilling of *Punc-17β* neurons (labeled by mCherry) does not affect neighboring D-type motor neurons labeled by *Punc-25-GFP*. DIC images show the same segment of ventral nerve cord as appeared in fluorescence images. (Scale bar, 10 μm.) (*B*) Photokilling of *Pnmr-1* neurons (labeled by mCherry) does not affect neighboring cells labeled by *Pglr-1-GFP*. AVB and other neurons labeled by *Pglr-1* but not by *Pnmr-1* are intact after light illumination. The positions of AVA (asterisk in cyan) and AVD (asterisk in white) are marked on images showing the animal before and after light illumination. (Scale bar, 10 μm.) (*C*) Plots of distribution of instantaneous locomotion speed when animals were transferred from food plate to food-free plate. Positive speed values reflect the forward motion, whereas negative speed values reflect the backward motion. When *Pnmr-1* cells were photokilled (*Upper*), the backward movement pattern was severely affected (Movie S6) and the speed was dramatically reduced (the curve shifts toward zero on the velocity axis). Ablation of *Pnmr-1* cells at young larval stage (L1) and late larval stage (L4) resulted in similar locomotion behaviors. When *Psra-11* cells were photokilled (*Lower*), the animals exhibit severely disrupted forward locomotion (Movie S8). At least 15 animals of each illumination condition were tracked and analyzed. (*D*) Temporally controlled motor neuron ablation by *Punc-17β-mito-miniSOG*. Schematic drawings show that *Punc-17β* labels DA and DB at L1. At late L1, VA and VB are born, such that *Punc-17β* labels DA, DB, VA, and VB from then on (*Top*). The DIC images show young adult transgenic animals that had been illuminated under blue light at young larval stage (L1) and late larval stage (L4), respectively (*Middle*). When illuminated at L1, the animals are severely uncoordinated and coil invariably toward the ventral side (arrowheads). When illuminated at L4, the worms are paralyzed and tend to coil toward the dorsal side (arrows). (*Bottom*) mCherry fluorescence images of animals having received light illumination. When illuminated at L1, DA and DB are ablated, and fluorescence disappears only in the dorsal cord (arrows). When illuminated at L4, animals lose not only DA and DB, but also VA and VB (arrowheads).

alone did not show any behavioral or cellular changes (Fig. 1*A*). The phototoxicity of miniSOG was specifically induced by blue light, as green light (560 ± 20 nm) caused no effects (Fig. 2*D*), consistent with the absorption spectrum of miniSOG. Moreover, expression of a miniSOG variant containing Cys426, which cannot divert light energy into $^1O_2$ generation (15), did not produce any fluorescence and was not able to kill cells (Fig. 1*A*; Table S1). miniSOG fused in-frame to the ACO-1 cytoplasmic aconitase produced limited damage that was not sufficient to kill cells (Fig. 1*A*; Table S1), consistent with the very short range of

$^1O_2$ (15) and the key role of mitochondria in triggering cell death. Among the different mitochondrial tags, targeting to the mitochondrial outer membrane using the N-terminal 55-amino-acid residues of TOMM-20 provided the most potent phototoxic effect (Fig. 1*A*; Table S1). We therefore focused on TOMM-20 (N′55aa)-miniSOG and hereafter refer to this as mito-miniSOG.

Cell Ablation by Mitochondrially Targeted miniSOG Is Light-Dose-Dependent and Enhanced by Pulse Illumination. We empirically determined that the effectiveness of cell ablation with mitochondrially targeted miniSOG (mito-miniSOG) correlated with whether green fluorescence of miniSOG was visually detectable under a standard epi-fluorescence compound microscope (*SI Materials and Methods*). We also tested how the light dosage might affect the effectiveness of cell ablation. mito-miniSOG–induced ablation of the ventral cord A- and B-type motor neurons resulted in paralysis (Fig. 2*C*; Movies S1 and S2). We analyzed the percentage of paralyzed animals expressing *Punc-17β-mito-miniSOG* following various time periods of continuous blue-light treatment and found that the paralysis increased with longer durations of light exposure (Fig. 2*D*). We also devised a repetitive pulsed blue lighting procedure (0.5 s light; 1.5 s dark) (*Materials and Methods*) and found that it resulted in three times more effective cell ablation, given the same intensity and total dose of blue-light illumination (Fig. 2*D*). Under pulsed blue-light exposure for a total of 15–30 min, the animals remained healthy and reproduced normally. Thus, photoablation effects by activated mito-miniSOG appear to be graded, and pulsed lighting can be advantageous. Further experimentation would be necessary to investigate why different regimens for delivering a given photon dose vary in effectiveness and whether the efficacy of cell killing can be further optimized.

Caspase *ced-3* Is Not Required for Cell Death Induced by mito-miniSOG. We wanted to gain clues as to whether mito-miniSOG–mediated cell killing involves known cell-death pathways. Two genes essential for apoptotic programmed cell death in *C. elegans* are the caspase *ced-3* and its activator *ced-4* (21). We found that null mutations of *ced-3* or *ced-4* did not block the photoablation of neurons expressing *Pnmr-1*– or *Punc-17β*–mito-miniSOG, as monitored by the disappearance of mCherry fluorescence or the defective locomotion behavior (Fig. 2*E*; Table S1). The phagocytic receptor *ced-1*, a homolog of the human CD91 and LRP proteins, acts in phagocytosis of both apoptotic cells and nonapoptotic debris (21, 22) and is also shown to up-regulate the unfolded protein response in *C. elegans* innate immunity (23). In a strong loss-of-function *ced-1* mutant, roughly 30–40% of *Pnmr-1-mito-miniSOG*–expressing cells retained normal expression of mCherry, with little morphological evidence of disintegration 16 h after light exposure (Fig. 2*E*). However, analysis of the locomotion speed of such animals showed that the *ced-1* mutation did not significantly alleviate the locomotion deficit resulting from ablation of *Pnmr-1* neurons by mito-miniSOG (Fig. S1). These data imply that clearance of the damaged cells caused by mito-miniSOG involves dedicated cellular pathways including *ced-1*. The above observations thus suggest that the mechanism of mito-miniSOG–induced cell death does not require the core programmed cell-death pathway and that phagocytosis of the damaged cells contributes to their elimination. It will be of future interest to investigate the mechanisms underlying miniSOG toxicity.

Activated mito-miniSOG Does Not Cause Cell-Nonautonomous Cytotoxicity. As dying cells may send damaging signals to other cells and cause nonautonomous consequences, we addressed whether miniSOG–induced cell death could affect the neighboring cells. *Punc-17β*–expressing cholinergic motor neurons in the ventral nerve cord are interdigitated with the GABAergic motor neurons, which express *Punc-25-GFP* (24, 25). Killing *Punc-17β*–expressing motor neurons by mito-miniSOG did not cause detectable abnormality of the neighboring GABAergic neurons (Fig. 3*A*). To test the cell-autonomous ablation in a more complex environment, we examined the interneurons that reside in the densely packed head ganglia. *Pnmr-1*–expressing neurons include four pairs of interneurons: AVA, AVE, AVD, and RIM (26). *Pglr-1-GFP* labels all of the *Pnmr-1*–expressing cells and additional adjacent neurons (26, 27). We generated a strain containing both *Pnmr-1-mito-miniSOG* and *Pglr-1-GFP*. When *Pnmr-1*–expressing neurons (marked by mCherry) were photokilled, the neighboring GFP-labeled cells showed normal morphology (Fig. 3*B*).

It remains possible that cell-nonautonomous damages might occur independently of morphological changes. To address this, we next examined the behavioral consequences of selective ablation of the premotor interneurons. *Pnmr-1*–expressing interneurons regulate backward locomotion (26, 28) and reside in the near neighborhood of the interneurons AVB, which regulate forward locomotion and express *Psra-11* (29). When worms are transferred from a plate with food to a plate without food, they display a dramatically changed locomotion pattern, characterized by high velocity and infrequent short reversals (26, 30). We tracked the locomotion speed and pattern of the animals before and after photoablation (*Materials and Methods*). The adult animals with *Pnmr-1* cells photo-ablated at L4 showed impaired backward locomotion (Fig. 3*C*; Movies S3, S4, S5, and S6) in a pattern similar to that of animals in which *Pnmr-1* cells were killed by either overexpression of the proapoptotic factor ICE (26) or laser ablation in L1 larvae (28). The sinusoidal pattern of the forward motion in these animals was largely normal, supporting that the AVB neurons were unharmed. We note that, despite the normal sinusoidal forward pattern, the animals with *Pnmr-1* cells ablated showed a modest and significant decrease in the locomotion speed (Fig. 3*C*; Fig. S1*B*), the underlying cause of which would be of future investigation. Conversely, when AVB neurons were ablated by *Psra-11-mito-miniSOG*, the forward sinusoidal locomotion pattern was severely disrupted (Fig. 3*C*; Movies S7 and S8). Nonetheless, these animals could drag along in a forward motion, suggesting that the pulling force may likely come from the head-and-neck motor system. The backward locomotion of the animals with *Psra-11* cells ablated was largely normal, indicating that AVA/AVD/AVE neurons were unharmed. Together, these data support that the mito-miniSOG–mediated cell ablation occurs in a cell-specific and autonomous manner.

Temporally Activated mito-miniSOG Selectively Ablates Motor Neurons Arising from Specific Stages. The light-inducible cell killing by mito-miniSOG offers an advantage for temporally controlled cell ablation. To explore such use, we illuminated the *Punc-17β-mito-miniSOG* animals at young (L1) and older (L4) larval stages. The *Punc-17β*–expressing DA and DB neurons are embryonically born and present in young L1, whereas the *Punc-17β*–expressing VA and VB neurons are born in late L1 and early L2 stages (Fig. 3*D*) (31). We observed that, following light illumination at the young L1 stage, the animals lacked mCherry-labeled processes from DA and DB in the dorsal nerve cord (Fig. 3*D*). Behaviorally, these animals displayed uncoordinated movement as they reached adult stages and coiled toward the ventral side (Fig. 3*D*), consistent with a lack of excitatory inputs from the DA and DB neurons to the dorsal body muscles. In contrast, when *Punc-17β-mito-miniSOG* animals were light-illuminated at L4 larval stage, all mCherry-labeled processes in the dorsal and ventral nerve cords disintegrated, and the animals displayed severe paralysis (Fig. 3*D*), consistent with the elimination of excitatory inputs to both ventral and dorsal body muscles. We also performed stage-specific ablation on the *Pnmr-1*–expressing interneurons, which are born during embryogenesis and persist through adulthood. We observed that killing *Pnmr-1* neurons in L1 and L4 animals resulted in a similar defective locomotion pattern (Fig. 3*C*, *Upper*). The latter analysis indicates that the *Pnmr-1* interneurons are required continuously throughout development to regulate locomotion speed. In all cases, mCherry did not reappear in the L1-illuminated worms when they reached adult stages, indicating that cell ablation is permanent.

Ablation of Premotor Interneurons Reveals a Role of the AVB Interneurons in the Convulsive Behavior of *acr-2(gf)* Mutants. As an application of the mito-miniSOG–induced cell ablation method in analyzing neural circuit function, we investigated the neural

control of the convulsive behavior caused by a gain-of-function mutation in *acr-2*. ACR-2 is a nicotinic acetylcholine receptor that is expressed in the ventral cord cholinergic B and A classes of motor neurons and functions in maintaining the excitability of these neurons (32). The *acr-2(gf)* mutation causes increased cholinergic transmission, and the mutant animals exhibit a severe disruption of undulatory locomotion accompanied with periodic seizure-like whole-body contraction (Fig. 4*B*). It is unclear how the convulsive events are initiated and regulated and whether the movement defect is the result of convulsion. The major neural inputs to the motor neurons are from the premotor interneurons AVB and PVC, which regulate the B class of motor neurons in forward locomotion, and from the premotor interneurons AVA, AVD, and AVE, which regulate the A class of motor neurons in backward locomotion (Fig. 4*A*) (28, 33). We therefore selectively ablated the premotor interneurons to address their roles in the convulsive behavior of *acr-2(gf)* mutants (Tables S1 and S2). When AVB neurons were ablated by *Psra-11-mito-miniSOG* in *acr-2(gf)* adult animals, the convulsion rates significantly decreased (Fig. 4*B*; Movies S9 and S10). In contrast, when the premotor *Pnmr-1*–expressing interneurons were killed by light illumination, the convulsion frequency of *acr-2(gf)* animals instead significantly increased (Fig. 4*B*; Movies S11 and S12). For comparison, we performed traditional laser ablation of AVB or AVA/AVD/AVE in L1 worms of *acr-2(gf)* and observed a similar suppression of the convulsion by killing AVB and an enhancement by killing AVA/AVD/AVE (Fig. 4*B*). These data indicate that AVB neurons positively regulate the convulsion events and suggest that the premotor interneurons AVA/AVD/AVE may impose a negative regulation on shrinking events through inhibiting AVB activity. Indeed, when we simultaneously ablated both *Pnmr-1* and *Psra-11* neurons, the convulsion frequency of *acr-2 (gf)* dropped to the same level as ablating *Psra-11* neurons alone. It is worth noting that ablation of the interneurons affected only the onset of convulsion events and did not alleviate the overall locomotion pattern defect of *acr-2(gf)* animals (Movies S9, S10, S11, S12, S13, and S14). Thus, it is the abnormal motor neuron activities caused by the ACR-2(gf) channel that account for the uncoordinated movement pattern in the mutants.

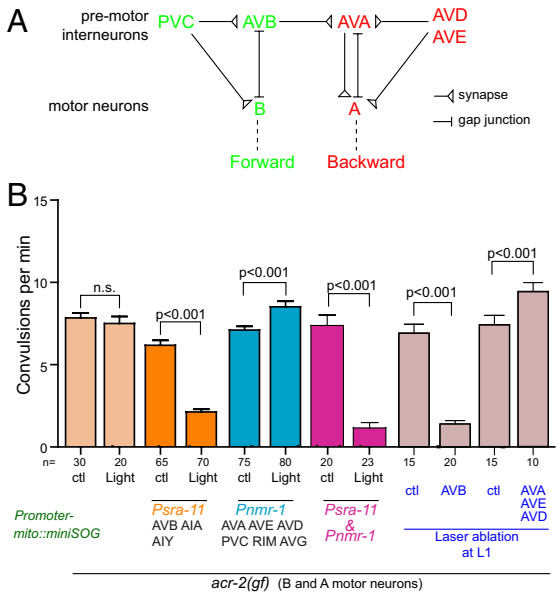

Fig. 4. Ablation of the premotor interneurons reveals their roles in the regulation of convulsions in *acr-2(gf)* animals. (*A*) Shown is the connectivity among premotor interneurons and ventral cord motor neurons that regulates forward and backward movement (based on refs. 25, 28, 33). (*B*) *acr-2 (gf)* animals exhibit periodic convulsions; frequency of convulsions (min^{-1}) in young adult animals are quantified in the graph. Ablation of specific subsets of premotor interneurons in young adult animals by activation of mito-miniSOG causes differential effects on convulsion. Ablating AVB results in a suppression of convulsive events, whereas ablating AVA and other backward premotor interneurons enhances the convulsive behavior. Control (ctl) groups are the same genotype without light illumination. Ablation of cells using both *Psra-11* and *Pnmr-1* together resulted in the decrease of convulsions frequency. Similar results are observed when AVB (labeled by *Psra-11-GFP*) or AVA, AVE, and AVD (labeled by *Pnmr-1-mCherry*) are killed by laser ablation at L1 stage. Control (ctl) groups are the animals of same genotype with laser aimed at the epidermis instead of mCherry-labeled neurons. Statistics used two-tailed Student's *t* test. Error bar shows SEM.

Discussion

We have reported a simple inducible cell ablation method in *C. elegans* using the genetically encoded singlet oxygen generator protein, miniSOG. We provide both morphological and behavioral evidence that photokilling of cells by targeting miniSOG to mitochondria is specific to the targeted cells and does not impose discernible damages on neighboring cells. We also show that photoablation by mito-miniSOG is effective in larval and adult stages and that the use of stable transgenic mito-miniSOG ensures the feasibility of comparing a large number of samples with a uniform standard. In comparison with the traditional laser-killing methodology (35), photoablation by mito-miniSOG requires only a standard fluorescent light source in setup and does not need extensive anatomical expertise. Moreover, laser killing of neurons is usually performed only in young L1 larvae because the body depth of older larvae and adults increases considerably, precluding precise focusing of a laser beam on targeting cells. It is also known that neuronal processes may remain intact even when the nucleus is eliminated by laser and could provide unknown function (35). We have shown that ablation by mito-miniSOG causes a complete disintegration, followed by clearance, of the dying cells. Current transgenic cell ablation methodologies in *C. elegans* predominantly rely on the constitutive expression of toxic proteins or caspases (36). Depending on the expression timing and strength of the promoters, these methods may often result in ablation of precursor cells or incomplete killing. Thus, mito-miniSOG–mediated cell ablation offers better temporal and spatial control in desired developmental and adult stages. We envision a particular advantage of mito-miniSOG in its application to our understanding of neuronal functions in aged adult animals.

In the course of developing the method of selective cell ablation using mito-miniSOG, we have also analyzed the roles of the premotor interneurons in regulating locomotion behaviors. The functions of these neurons have long been inferred from the wiring diagram (33) and were partly supported by early laser ablation experiments (28). Numerous investigators have recently revisited the roles of these neurons in locomotion by using a combination of laser ablation, genetic mutations, and optogenetic manipulations (30, 34, 37, 40). The laser ablations were performed in L1 larvae, and the animal behaviors were examined in adults, leaving the possibility that loss of the neurons might be compensated during animal growth. Although we cannot make precise parallel comparisons for the locomotion speed and pattern with those reported by other investigators, our observations that ablation of AVB leads to a severe disruption of the forward locomotion and that ablation of AVA/AVD/AVE causes a loss of the backward movement are consistent with the conclusions drawn in the recently published studies (34, 37, 40). Because we ablated these interneurons in adult animals, our studies provide evidence that the behavior deficits are direct consequences of the loss of these neurons. Furthermore, from our understanding of the convulsion behaviors of *acr-2(gf)* animals, we have identified an essential connection between the onset of convulsion and the forward locomotor motor system controlled by the premotor interneurons AVB. Unexpectedly, we found that the removal of AVA/AVD/AVE by mito-miniSOG or by laser ablation can enhance the convulsion frequency. We infer from this observation a negative feed-forward pathway from these neurons onto the AVB neurons. This is supported by our data that indicate simultaneous loss of both AVB and AVA/AVD/AVE results in a similar effect as the ablation of AVB alone. Our interpretation

is also consistent with the recent report showing that in the gap junction mutants, elevated AVA activity is associated with decreased activity in AVB (37). Because there are no extensive synaptic or gap junctions from the backward- to the forward-regulating premotor interneurons (33), these results raise important questions for the ongoing understanding of motor circuit modulation. Increasing studies have elegantly shown the power of optogenetic manipulations and optic imaging in dissecting the neural basis of behaviors in living animals (34, 37, 40). In conjuncture with these tools, the inducible and selective cell ablation by miniSOG will prove to be valuable in understanding neuronal function.

Various constitutive and inducible cell-ablation methods have been used in many cellular manipulations (1–8, 12). It may be difficult to accurately compare the efficiency of various genetically encoded cell-killing reagents as it requires knowledge of the protein concentration in vivo. The reconstituted caspase-mediated cell ablation method offers selective killing when the two halves of caspases are coexpressed in the same cell (36). However, variations in the expression levels driven by different promoters can often cause inconsistent cell ablations. Use of diphtheria toxin A for cell killing in *C. elegans* can also be problematic due to its high toxicity. The phototoxic protein KillerRed, developed from a red chromoprotein homolog of GFP, has been used to kill cultured cells when targeted to mitochondria, membranes, or histones and illuminated with green light (12, 38). KillerRed works through generation of radicals or hydrogen peroxide rather than through singlet oxygen (15, 39). miniSOG has an additional advantage for tagging functional proteins because it is a monomer less than one quarter the size of the obligate dimer of KillerRed (12, 15). In any case, the availability of two nonhomologous phototoxic proteins using different wavelengths and generating different reactive intermediates will add versatility to the optogenetic toolbox. We have previously suggested that miniSOG may also be targeted to other cellular compartments to allow mechanistic dissection of oxidative injury (15). The application of miniSOG presented here and its extended use in the future should greatly benefit functional studies in biology and clinical therapy.

Materials and Methods

Genetics and Molecular Biology and Transgenes. *C. elegans* strains were grown following standard procedure and animals were handled under ambient light unless noted. Strains and genotypes are shown in Table S1. All expression constructs are described in Table S2.

Photo Illumination. We used an upright Zeiss Axioplan 2 microscope equipped with an X-Cite 120 series fluorescence illumination lamp. Plates containing worms were placed, without any covers, on the stage with the blue light passing through without an objective lens. For light illumination, we restricted worms by placing a ring of filter paper soaked with 100 mM $CuCl_2$ with a hole of 15-mm diameter, about the size of the light illumination spot. The opening was spread with OP50 paste, and animals were placed on the food. Animals were exposed to either continuous blue light or pulse blue light (0.5 s on, 1.5 s off). The blue light (475 ± 20 nm) intensity that worms received was measured as 57 mW/cm^2. We used a Uniblitz unit (VMM-D1) to control the shutter (30 mm W/HS, LUDL Electronics).

Behavioral Analysis and Quantification of Convulsion. We used Worm Tracker 2.0 to track locomotion (see *SI Materials and Methods*). Quantification of convulsion was as described (32).

ACKNOWLEDGMENTS. We thank Suk-Ryool Kang for help in modifying tracker software; Claudiu Giurumescu for help in light control; and S. Cherra, N. Liu, A. D. Chisholm, and our laboratory members for comments. We thank Oliver Hobert, Villu Maricq, and Kenneth Miller for promoter constructs. This work was supported by National Institutes of Health Grants R01 NS035546 (to Y.J.) and R01 GM086197 (to R.Y.T.). Y.J. and R.Y.T. are Investigators of the Howard Hughes Medical Institute.

1. Miura M, Zhu H, Rotello R, Hartwieg EA, Yuan J (1993) Induction of apoptosis in fibroblasts by IL-1 beta-converting enzyme, a mammalian homolog of the C. elegans cell death gene ced-3. *Cell* 75:653–660.
2. Hong K, Driscoll M (1994) A transmembrane domain of the putative channel subunit MEC-4 influences mechanotransduction and neurodegeneration in C. elegans. *Nature* 367:470–473.
3. Palmiter RD, et al. (1987) Cell lineage ablation in transgenic mice by cell-specific expression of a toxin gene. *Cell* 50:435–443.
4. Breitman ML, et al. (1987) Genetic ablation: Targeted expression of a toxin gene causes microphthalmia in transgenic mice. *Science* 238:1563–1565.
5. Kobayashi K, et al. (1995) Immunotoxin-mediated conditional disruption of specific neurons in transgenic mice. *Proc Natl Acad Sci USA* 92:1132–1136.
6. Curado S, et al. (2007) Conditional targeted cell ablation in zebrafish: A new tool for regeneration studies. *Dev Dyn* 236:1025–1035.
7. Pisharath H, Rhee JM, Swanson MA, Leach SD, Parsons MJ (2007) Targeted ablation of beta cells in the embryonic zebrafish pancreas using E. coli nitroreductase. *Mech Dev* 124:218–229.
8. Saito M, et al. (2001) Diphtheria toxin receptor-mediated conditional and targeted cell ablation in transgenic mice. *Nat Biotechnol* 19:746–750.
9. Orrenius S, Gogvadze V, Zhivotovsky B (2007) Mitochondrial oxidative stress: Implications for cell death. *Annu Rev Pharmacol Toxicol* 47:143–183.
10. Agostinis P, et al. (2011) Photodynamic therapy of cancer: An update. *CA Cancer J Clin* 61:250–281.
11. Tour O, Meijer RM, Zacharias DA, Adams SR, Tsien RY (2003) Genetically targeted chromophore-assisted light inactivation. *Nat Biotechnol* 21:1505–1508.
12. Bulina ME, et al. (2006) A genetically encoded photosensitizer. *Nat Biotechnol* 24: 95–99.
13. Marek KW, Davis GW (2002) Transgenically encoded protein photoinactivation (FlAsH-FALI): Acute inactivation of synaptotagmin I. *Neuron* 36:805–813.
14. Teh C, et al. (2010) Optogenetic in vivo cell manipulation in KillerRed-expressing zebrafish transgenics. *BMC Dev Biol* 10:110.
15. Shu X, et al. (2011) A genetically encoded tag for correlated light and electron microscopy of intact cells, tissues, and organisms. *PLoS Biol* 9:e1001041.
16. Neupert W (1997) Protein import into mitochondria. *Annu Rev Biochem* 66:863–917.
17. Abe Y, et al. (2000) Structural basis of presequence recognition by the mitochondrial protein import receptor Tom20. *Cell* 100:551–560.
18. Watanabe S, et al. (2011) Protein localization in electron micrographs using fluorescence nanoscopy. *Nat Methods* 8:80–84.
19. Gardner PR, Fridovich I (1991) Superoxide sensitivity of the Escherichia coli aconitase. *J Biol Chem* 266:19328–19333.
20. Gourley BL, Parker SB, Jones BJ, Zumbrennen KB, Leibold EA (2003) Cytosolic aconitase and ferritin are regulated by iron in Caenorhabditis elegans. *J Biol Chem* 278:3227–3234.
21. Conradt B, Xue D (2005) Programmed cell death. *WormBook* :1–13.
22. Mangahas PM, Zhou Z (2005) Clearance of apoptotic cells in Caenorhabditis elegans. *Semin Cell Dev Biol* 16:295–306.
23. Haskins KA, Russell JF, Gaddis N, Dressman HK, Aballay A (2008) Unfolded protein response genes regulated by CED-1 are required for Caenorhabditis elegans innate immunity. *Dev Cell* 15:87–97.
24. Jin Y, Jorgensen E, Hartwieg E, Horvitz HR (1999) The Caenorhabditis elegans gene unc-25 encodes glutamic acid decarboxylase and is required for synaptic transmission but not synaptic development. *J Neurosci* 19:539–548.
25. White JG, Southgate E, Thomson JN, Brenner S (1976) The structure of the ventral nerve cord of Caenorhabditis elegans. *Philos Trans R Soc Lond B Biol Sci* 275:327–348.
26. Zheng Y, Brockie PJ, Mellem JE, Madsen DM, Maricq AV (1999) Neuronal control of locomotion in C. elegans is modified by a dominant mutation in the GLR-1 ionotropic glutamate receptor. *Neuron* 24:347–361.
27. Maricq AV, Peckol E, Driscoll M, Bargmann CI (1995) Mechanosensory signalling in C. elegans mediated by the GLR-1 glutamate receptor. *Nature* 378:78–81.
28. Chalfie M, et al. (1985) The neural circuit for touch sensitivity in Caenorhabditis elegans. *J Neurosci* 5:956–964.
29. Wenick AS, Hobert O (2004) Genomic cis-regulatory architecture and trans-acting regulators of a single interneuron-specific gene battery in C. elegans. *Dev Cell* 6:757–770.
30. Gray JM, Hill JJ, Bargmann CI (2005) A circuit for navigation in Caenorhabditis elegans. *Proc Natl Acad Sci USA* 102:3184–3191.
31. Sulston JE (1976) Post-embryonic development in the ventral cord of Caenorhabditis elegans. *Philos Trans R Soc Lond B Biol Sci* 275:287–297.
32. Jospin M, et al. (2009) A neuronal acetylcholine receptor regulates the balance of muscle excitation and inhibition in Caenorhabditis elegans. *PLoS Biol* 7:e1000265.
33. White JG, Southgate E, Thomson JN, Brenner S (1986) The structure of the nervous system of the nematode Caenorhabditis elegans. *Philos Trans R Soc Lond B Biol Sci* 314:1–340.
34. Piggott BJ, Liu J, Feng Z, Wescott SA, Xu XZ (2011) The neural circuits and synaptic mechanisms underlying motor initiation in C. elegans. *Cell* 147:922–933.
35. Fang-Yen C, Gabel CV, Samuel AD, Bargmann CI, Avery L (2012) Laser microsurgery in Caenorhabditis elegans. *Methods Cell Biol* 107:177–206.
36. Chelur DS, Chalfie M (2007) Targeted cell killing by reconstituted caspases. *Proc Natl Acad Sci USA* 104:2283–2288.
37. Kawano T, et al. (2011) An imbalancing act: Gap junctions reduce the backward motor circuit activity to bias C. elegans for forward locomotion. *Neuron* 72:572–586.
38. Waldeck W, et al. (2009) Autofluorescent proteins as photosensitizer in eukaryontes. *Int J Med Sci* 6:365–373.
39. Vegh RB, et al. (2011) Reactive oxygen species in photochemistry of the red fluorescent protein "Killer Red". *Chem Commun (Camb)* 47:4887–4889.
40. Faumont S, et al. (2011) An image-free opto-mechanical system for creating virtual environments and imaging neuronal activity in freely moving *Caenorhabditis elegans*. *PLoS One* 6(9):e24666.

Supporting Information

Qi et al. 10.1073/pnas.1204096109

SI Materials and Methods

Photo Illumination. Moderate expression of mitochondrially targeted mini singlet oxygen generator (mito-miniSOG) is the key for effective cell ablation, with minimal damages to the function of the cell. The green fluorescence from transgenic mito-miniSOG should be visually detectable under a standard epi-fluorescence microscope (10× eye pieces and 63× objectives). However, high expression levels of mito-miniSOG that can be detected under 10× objectives or under a standard GFP dissecting scope are usually unnecessary. We generally maintained mito-miniSOG transgenic animals in standard incubators and would advise to take caution in keeping animals away from continuous room-light exposure.

After light illumination, worms were transferred to freshly seeded plates before any analysis. The effectiveness of photokilling was scored by imaging and behavioral analysis. In practice, we recommend that the time of light illumination should be determined empirically with respect to the specific microscopes and light sources and the transgenes.

Laser Ablation. Young L1 worms were anesthetized by 1% 1-phenoxy-2-propanol and placed on an agar pad under a cover glass. The laser setup and operation were essentially described in previous studies (1). In this experiment, 120 mW of laser power and two pulses of 4 ms/pulse were used once the laser was aimed on the target cells.

Imaging. For fluorescent imaging, animals were anesthetized in 0.6% 1-phenoxy-2-propanol, and images were captured on a Zeiss LSM510 confocal microscope. For bright-field images of worms, the plates were placed on ice until the worms stopped moving. Images were acquired under a Zeiss fluorescence stereo microscope (Discovery V12) using a Nikon camera (DS.Qi1Mc).

Behavioral Analysis. For strains expressing miniSOG constructs under the *unc-17β*, *unc-25*, or *acr-2* promoters, the effectiveness of photokilling was scored on the basis of the degree of paralysis or uncoordination observed among a group of 20–30 animals ~16 h following light exposure.

We used Worm Tracker 2.0 to track locomotion (W. Schafer's laboratory, MRC Laboratory of Molecular Biology, Cambridge, United Kingdom) (2). To prepare the tracking plate, unseeded NGM plates were warmed up to room temperature. Immediately before transferring the worms, about 500 μL of 100 mM $CuCl_2$ was poured and swirled on the rim of the plate to form a "copper ring," and excessive $CuCl_2$ solution was removed. Individual young adults on an OP50 lawn were gently transferred to M9 in a scooping motion using a wet flattened platinum wire tip. An aspiration micropipette was used to rinse off any bacteria. The worm was then transferred onto a fresh tracking plate using the same micropipette. The plate was placed on the tracker platform. The tracking started about 1 min after the puddle of M9 with the worm was absorbed into the agar and the worm had started crawling. Each tracking movie lasted 5 min with 10 frames per second. Movies were analyzed using the algorithms modified by Suk-Ryool Kang (Department of ECE, University of California, San Diego). The reversal events induced by encountering the copper ring were manually removed from the analysis.

1. Wu Z, et al. (2007) Caenorhabditis elegans neuronal regeneration is influenced by life stage, ephrin signaling, and synaptic branching. *Proc Natl Acad Sci USA* 104: 15132–15137.

2. Ben Arous J, Tanizawa Y, Rabinowitch I, Chatenay D, Schafer WR (2010) Automated imaging of neuronal activity in freely behaving Caenorhabditis elegans. *J Neurosci Methods* 187:229–234.

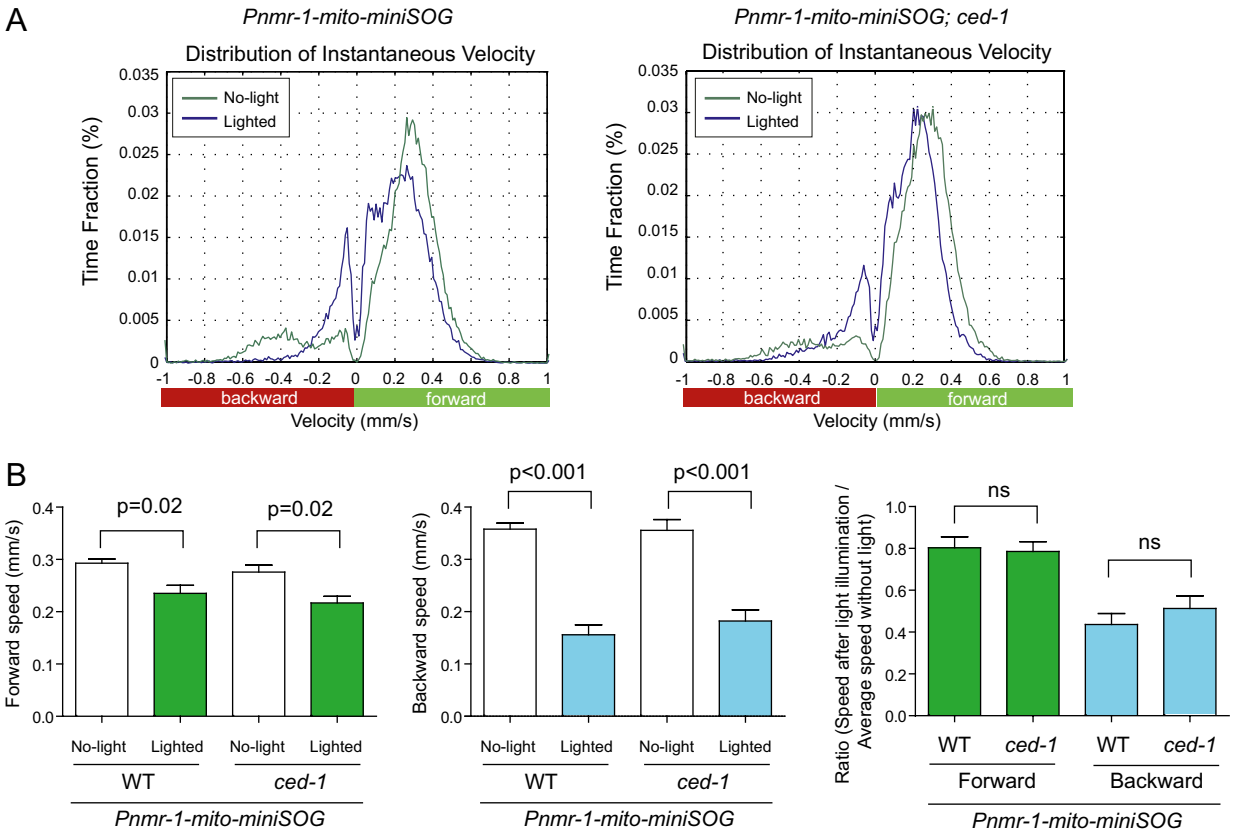

Fig. S1. *ced-1* does not alleviate the behavior deficit caused by ablating *Pnmr-1* cells using mito-miniSOG. (*A*) Plots of distribution of instantaneous locomotion speed when animals were transferred from food plate to food-free plate. When *Pnmr-1* cells were photokilled, the backward locomotion was severely defective; the locomotion speed of backward movements decreased dramatically on the plot. Ablation of *Pnmr-1* cells in *ced-1* results in similar backward-movement defects. (*B*) Quantification of the locomotion speed in forward (*Left*) and backward (*Center*) movement in animals with or without light illumination. The speed changes resulting from the light illumination were quantified (*Right*). Statistics used the two-tailed Student's *t* test. Error bar shows SEM.

Table S1. Strains and phenotypes after blue-light illumination

Construct type	Strain	Genotype	Killing effectiveness	Behavior after photo illumination
free miniSOG	CZ13035	*Pacr-2-miniSOG(juEx3136)*	No cells killed	Superficially wild type
	CZ15282	*Punc-17β-miniSOG; Pttx-3-RFP(juEx4205)*	No cells killed	Superficially wild type
	CZ15280	*Pnmr-1-miniSOG; Pnmr-1-mCherry(juEx4203)*	No cells killed	Superficially wild type
hCOX-8N-miniSOG	CZ13024	*Pacr-2-COX8N::miniSOG(juEx3126)*	*	Paralyzed
	CZ15169	*Pnmr-1-COX8N::miniSOG; Pnmr-1-mcherry(juEx4119)*	*	Slow forward movement, slow and defective backward movement, loss of posterior touch response
	CZ14120	*Psra-11-COX8N::miniSOG; Psra-11-mCherry(juEx3593)*	†	Mildly uncoordinated
	CZ11947	*Prgef-1-COX8N::miniSOG(juEx2702)*	‡	Paralyzed, inactive
	CZ11886	*Punc-25-COX8N::miniSOG(juEx2673)*	*	Moderately uncoordinated
	CZ12041	*Punc-25-GFP(juIs76) II ; Punc-25-COX8N::miniSOG(juEx2752)*	*	NA
aco-1-miniSOG	CZ14480	*Pnmr-1-aco-1::miniSOG; Pnmr-1-mCherry(juEx3773)*	No cells killed	Superficially wild type
aco-2-miniSOG	CZ15171	*Pnmr-1-aco-2::miniSOG; Pnmr-1-mCherry(juEx4121)*	*	Slow forward movement, slow and defective backward movement, loss of posterior touch response
	CZ14874	*Psra-11-aco-2::miniSOG; Psra-11-mCherry(juEx3959)*	*	Uncoordinated and unsustained forward movement
tomm-20-miniSOG	CZ14476	*Pnmr-1-tomm-20::miniSOG; Pnmr-1-mCherry(juEx3769)*	‡	Slow forward movement, slow and defective backward movement, loss of posterior touch response
tomm-20-N′55AA-miniSOG (mito-miniSOG)	CZ14478	*Pnmr-1-tomm-20N::miniSOG; Pnmr-1-mCherry(juEx3771)*	§	Slow forward movement, slow and defective backward movement, loss of posterior touch response
	CZ15166	*Psra-11-tomm-20-N::miniSOG; Psra-11-mcherry(juEx3802)*	§	Uncoordinated and unsustained forward movement, severely defective sinusoidal forward pattern
	CZ14527	*Punc-17β- tomm-20N::miniSOG(juEx3790)*	§	Paralyzed
	CZ15033	*Punc-25-GFP(juIs76); punc-17β -tomm-20N::miniSOG (juEx4064)*	§	Paralyzed
	CZ14627	*Pglr-1-GFP(nuIs1); Pnmr-1-tomm-20N::miniSOG; Pnmr-1-mCherry(juEx3771)*	§	Slow forward movement, slow and defective backward movement, loss of posterior touch response
	CZ15167	*Pglr-1-tomm-20N::miniSOG; Pnmr-1-mCherry(juEx3955)*	§	Slow and uncoordinated forward movement; kinky, very slow, and severely uncoordinated backward movement; loss of posterior touch response
tomm-20-N′55AA-miniSOG (Gly426Cys)	CZ15290	*Pnmr-1-tomm-20 N′55AA::miniSOG(426C); Pnmr-1-mcherry(juEx4213)*	No cells killed	No green fluorescence; superficially wild type
	CZ15286	*Punc-17β -tomm-20 N′55AA::miniSOG(426C)(juEx4209)*	No cells killed	No green fluorescence; superficially wild type
tomm-20-N′55AA-GFP	CZ15288	*Pnmr-1-tomm-20N::GFP; Pnmr-1-mCherry(juEx4211)*	No cells killed	Superficially wild type
	CZ15284	*Punc-17β-tomm-20N::GFP; Pttx-3-RFP(juEx4207)*	No cells killed	Superficially wild type
tomm-20-N′55AA-miniSOG	CZ14879	*ced-3(n717) IV ; Pnmr-1-tomm-20N::miniSOG; Pnmr-1-mCherry(juEx3771)*	§	Slow forward movement, slow and defective backward movement, loss of posterior touch response
	CZ14805	*ced-3(n717) IV dpy-4(e1166) IV ; Pnmr-1-tomm-20N::miniSOG; Pnmr-1-mCherry(juEx3771)*	§	Slow forward movement, slow and defective backward movement, loss of posterior touch response
	CZ14878	*ced-3(ok2734) IV ; Punc-17(beta)- tomm-20N::miniSOG(juEx3790)*	§	Paralyzed
	CZ15132	*ced-4(n1162) III ; Pnmr-1-tomm-20N::miniSOG; Pnmr-1-mCherry(juEx3771)*	§	Slow forward movement, slow and defective backward movement, loss of posterior touch response
	CZ15275	*ced-1(e1735) I ; Pnmr-1-tomm-20(N′-55AA)::miniSOG; Pnmr-1-mCherry(juEx3771)*	‡	Slow forward movement, slow and defective backward movement, loss of posterior touch response
tomm-20-N′55AA-miniSOG	CZ14571	*acr-2(n2420) X ; Psra-11-tomm-20-N′55AA::miniSOG; Psra-11-mcherry(juEx3802)*	§	Convulsion reduced
	CZ14569	*acr-2(n2420) X ; Pnmr-1-tomm-20 N′55AA::miniSOG; Pnmr-1-mCherry(juEx3800)*	§	Convulsion enhanced

Table S1. Cont.

Construct type	Strain	Genotype	Killing effectiveness	Behavior after photo illumination
	CZ16539	*acr-2(n2420) X ; Psra-11-tomm-20 N'55AA::miniSOG; Psra-11-mCherry; Pnmr-1-tomm-20 N'55AA::miniSOG; Pnmr-1-mCherry(juEx4817)*	[§]	Convulsion reduced
NA	CZ10402	*acr-2(n2420) X*	NA	NA (as control)
	CZ14166	*acr-2(n2420) X ; Psra-11-gfp(juEx3603)*	NA	NA (used in laser ablation)
	CZ10733	*acr-2(n2420) X ; Pnmr-1-mCherry(juEx2324)*	NA	NA (used in laser ablation)

hCOX8N: N terminus 29AA of human *COX8a*; *tomm-20*: full-length *C. elegans tomm-20*; *tomm-20N*: N terminus 55AA of *C. elegans tomm-20*; *aco-1*: full-length *C. elegans aco-1*, cytoplasmic aconitase; *aco-2*: full-length genomic DNA of *C. elegans aco-2*, mitochondria aconitase. NA, not applicable.
*Mildly effective (10–50%).
[†]Marginally effective (0–10%).
[‡]Moderately effective (50–85%).
[§]Highly effective (85–100%).

Table S2. DNA constructs information

Plasmid no.	Description	Cloning details
pCZGY#1232	miniSOG in pENTR[1-2]	Full-length miniSOG was amplified from pcDNA3.1H_H2B_miniSOG-IRES-mCherry (1).
pCZGY#1026	COX8aN::miniSOG in pENTR[1-2]	N-terminal 29-amino-acid residue of human COX8a was fused in front of miniSOG (1).
pCZGY#1533	tomm-20::miniSOG in pENTR[1-2]	*C. elegans* tomm-20 full-length cDNA was generated by RT-PCR from total RNA. Acc III was added before the stop codon and used to insert miniSOG.
pCZGY#1534	tomm-20N::miniSOG in pENTR[1-2]	N-terminal 55-amino-acid residue of *C. elegans* tomm-20 was generated by RT-PCR from total RNA. A stop codon was added in the 3′ reverse primer. Acc III was added in front of the stop codon and used to insert miniSOG.
pCZGY#1536	aco-1::miniSOG in pENTR[1-2]	*C. elegans* aco-1 cDNA was generated by RT-PCR from total RNA. Age I was added in front of the stop codon, and miniSOG was cloned into the Age I site via Acc III.
pCZGY#1563	aco-2::minSOG in pENTR[1-2]	*C. elegans* aco-2 genomic DNA (F54H12.1c.1) was amplified by PCR from worm genomic DNA. Age I was added in front of the stop codon. miniSOG was cloned into Age I site via Acc III.
pCZGY#1703	tomm-20N::miniSOG(426Cys) in pENTR[1-2]	Gly426 of tomm-20N::miniSOG in pCZGY#1533 was mutated to Cys426 via PCR cloning.
pCZGY#1614	tomm-20N::GFP in pENTR[1-2]	miniSOG in pCZGY#1534 was replaced by GFP from vector pPD96.75 via Acc III.
pCZGY#902	Pnmr-1 in pDEST[R1-R2]	1,078-bp upstream genomic sequences of *nmr-1* were PCR-cloned from worm genomic DNA.
pCZGY#1091	Punc-17-beta in pDEST[R1-R2]	Vector contains two fragments of regulatory sequence upstream of unc-17. The promoter was PCR-cloned from Punc-17B:unc-31 (2). This promoter is expressed only in A- and B-type motor neurons.
pCZGY#1541	Psra-11 (promoter A) in pDEST[R1-R2]	Vector contains 4,550-bp upstream regulatory sequences of *sra-11*. The promoter was subcloned from pOH149 (3).
pCZGY#835	Pacr-2 in pDEST[R1-R2]	Vector contains 1,888-bp upsteam regulatory sequences of *acr-2*. The promoter was PCR-cloned from *C. elegans* genomic DNA.
pCZGY#66	Prgef-1 in pDEST[R1-R2]	Vector contains 3,466-bp upsteam regulatory sequences of *rgef-1*. The promoter was PCR-cloned from *C. elegans* genomic DNA.
pCZGY#1567	Pglr-1 in pDEST[R1-R2]	Vector contains 2,826-bp upstream regulatory sequences of *glr-1*. The promoter was subcloned from pDM1286 Pglr-1::GFP (4).
pCZGY#836	Punc-25 in pDEST[R1-R2]	Vector contains 1,946-bp upstream regulatory sequences of *unc-25*, amplified from *C. elegans* genomic DNA.

1. Shu X, et al. (2011) A genetically encoded tag for correlated light and electron microscopy of intact cells, tissues, and organisms. *PLoS Biol* 9(4):e1001041.
2. Charlie NK, Schade MA, Thomure AM, Miller KG (2006) Presynaptic UNC-31 (CAPS) is required to activate the G alpha(s) pathway of the *Caenorhabditis elegans* synaptic signaling network. *Genetics* 172(2):943–961.
3. Wenick AS, Hobert O (2004) Genomic cis-regulatory architecture and transacting regulators of a single interneuron-specific gene battery in C. elegans. *Dev Cell* 6(6):757–770.
4. Zheng Y, Brockie PJ, Mellem JE, Madsen DM, Maricq AV (1999) Neuronal control of locomotion in C. elegans is modified by a dominant mutation in the GLR-1 ionotropic glutamate receptor. *Neuron* 24(2):347–361.

Movie S1. *Punc-17β-mito-miniSOG*. Nonlighted control. These transgenic young adult animals did not receive blue-light illumination and move superficially as wild type.

Movie S1

Movie S2. *Punc-17β-mito-miniSOG*. Lighted. These transgenic animals received blue-light illumination at L4 and were videotaped at the young adult stage. They are completely paralyzed.

Movie S2

Movie S3. *Pnmr-1-mito-miniSOG*. Nonlighted control. Forward motion. These transgenic young adult animals did not receive blue-light illumination and move forward as wild type.

Movie S3

Movie S4. *Pnmr-1-mito-miniSOG*. Lighted. Forward motion. These transgenic animals received blue-light illumination at L4 and were videotaped at the young adult stage. They show a largely normal sinusoidal forward-locomotion pattern but slow speed.

Movie S4

Movie S5. *Pnmr-1-mito-miniSOG*. Nonlighted control. Backward motion. These transgenic young adult animals did not receive blue-light illumination and move backward as wild type.

Movie S5

Movie S6. *Pnmr-1-mito-miniSOG*. Lighted. Backward motion. These transgenic animals received blue-light illumination at L4 and were videotaped at the young adult stage. They can initiate the backward movement, but the locomotion is very defective.

Movie S6

Movie S7. *Psra-11-mito-miniSOG*. Nonlighted control. These transgenic young adult animals did not receive blue-light illumination. The movie shows moments of both forward and backward locomotion, which is superficially wild type.

Movie S7

Movie S8. *Psra-11-mito-miniSOG*. Lighted. These transgenic animals received blue-light illumination at L4 and were videotaped at the young adult stage. The movie shows moments of both forward and backward locomotion. The worms can barely move forward; the backward movement is largely reserved.

Movie S8

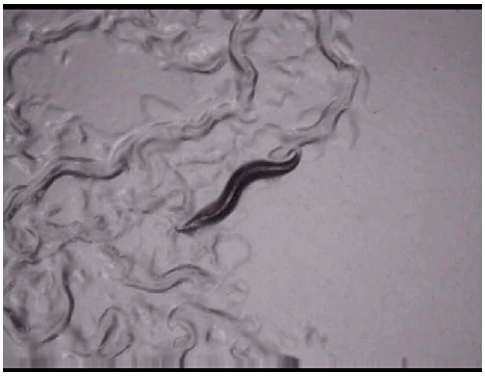

Movie S9. *Psra-11-mito-miniSOG; acr-2(gf)*. Nonlighted control. These transgenic young adult animals show convulsive behaviors, as *acr-2(gf)* alone.

Movie S9

Movie S10. *Psra-11-mito-miniSOG; acr-2(gf)*. Lighted. These transgenic animals received blue-light illumination at L4 and were videotaped at the young adult stage. The convulsion frequency is significantly reduced.

Movie S10

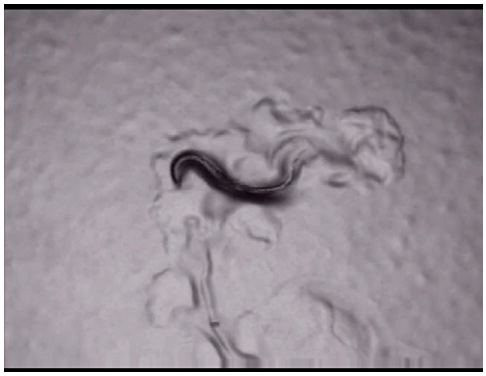

Movie S11. *Pnmr-1-mito-miniSOG; acr-2(gf)*. Nonlighted control. These transgenic young adult animals show convulsive behaviors, as *acr-2(gf)* alone.

Movie S11

Movie S12. *Pnmr-1-mito-miniSOG; acr-2(gf)*. Lighted. These transgenic animals received blue-light illumination at L4 and were videotaped at the young adult stage. The convulsion frequency is significantly increased.

Movie S12

Movie S13. *Psra-11-mito-miniSOG; Pnmr-1-mito-miniSOG; acr-2(gf).* Nonlighted control. These transgenic young adult animals show convulsive behaviors, as *acr-2(gf)* alone.

Movie S13

Movie S14. *Psra-11-mito-miniSOG; Pnmr-1-mito-miniSOG; acr-2(gf).* Lighted. These transgenic animals received blue-light illumination at L4 and were videotaped at the young adult stage. The convulsion frequency is significantly reduced.

Movie S14